Biogeosciences Discuss., 11, 12871–12893, 2014
www.biogeosciences-discuss.net/11/12871/2014/
doi:10.5194/bgd-11-12871-2014

Biogeosciences Discussions
Open Access

Space-time variability of alkalinity in the Mediterranean Sea

G. Cossarini, P. Lazzari, and C. Solidoro

Istituto Nazionale di Oceanografia e di Geofisica Sperimentale, Sgonico (Trieste), Italy

Received: 1 August 2014 – Accepted: 20 August 2014 – Published: 3 September 2014

Correspondence to: G. Cossarini (gcossarini@ogs.trieste.it)

Published by Copernicus Publications on behalf of the European Geosciences Union.

Abstract

The paper provides a basin assessment of the spatial distribution of ocean alkalinity in the Mediterranean Sea. The assessment is made using a 3-D transport-biogeochemical-carbonate model to integrate the available experimental findings, which also constrains model output.

The results indicate that the Mediterranean Sea shows alkalinity values that are much higher than those observed in the Atlantic Ocean on a basin-wide scale. A marked west-to-east surface gradient of alkalinity is reproduced as a response to the terrestrial discharges, the mixing effect with the Atlantic water entering from the Gibraltar Strait and the Black Sea water from Dardanelles, and the surface flux of evaporation minus precipitation. Dense water production in marginal seas (Adriatic and Aegean Seas), where alkaline inputs are relevant, and the Mediterranean thermohaline circulation sustains the west-to-east gradient along the entire water column. In the surface layers, alkalinity has a relevant seasonal cycle (up to 40 $\mu mol\,kg^{-1}$) that is driven both by physical and biological processes. A comparison of alkalinity vs. salinity indicates that different regions present different relationships. In regions of freshwater influence, the two measures are negatively correlated due to riverine alkalinity input, whereas they are positively correlated in open seas. Alkalinity always is much higher than in the Atlantic waters, which might indicate a higher than usual buffering capacity towards ocean acidification, even at high concentrations of dissolved inorganic carbon.

1 Introduction

The dissolution of atmospheric CO_2 mitigates the effects of the atmospheric concentration of fossil carbon emissions but causes acidification in marine water. Experimental observations of ocean acidification have already been recorded, and evidence suggests that this phenomenon is occurring at an unprecedented rate. A number of studies indicate that ocean acidification might impact the structure and functioning of ecolog-

BGD
11, 12871–12893, 2014

ical systems, with cascading consequences on socio-economic activities (Rodrigues et al., 2013; Turley and Boot, 2011). Alkalinity, a measure of the capability of a solution to accept protons (Zeebe and Wolf-Gladrow, 2001), potentially buffers these effects. Different regional seas present different responses to global changes also as a consequence of specific alkalinity conditions. As an example, the Mediterranean Sea, a landlocked, relatively small, highly dynamic ecosystem with high anthropic pressure in coastal areas, calls for ad hoc studies. In fact, the few existing data indicate that in parallel with salinity, alkalinity is significantly higher in the whole Mediterranean Sea compared with the Atlantic Ocean, with an east-west spatial negative gradient. Thus, the alkalinity concentration increases moving from the Atlantic Ocean to the western basin of the Mediterranean and reaches its maximum values in the eastern basin (Schneider et al., 2007; Touratier and Goyet, 2011). This pattern clearly indicates that it is not possible to address the study of this basin by relying only on the results of global studies. Global climatology has been produced for pH and alkalinity (Lee et al., 2006), often based on the use of empirical site-specific regressions between alkalinity and temperature and salinity data. However, few data refer to the Mediterranean Sea, and as such, the statistical spatial interpolation and extrapolation of existing information are critical in this important basin.

In the open sea environment, alkalinity often correlates with salinity and temperature (Lee et al., 2006). The underpinning process is that evaporation and precipitation concentrate, or dilute, all compounds that contribute to alkalinity. The regression coefficients, however, change with the nature and relative composition of these compounds and can vary over different regions. However, these empirical relationships are widely used to reconstruct the spatio-temporal distribution of alkalinity from existing data sets and to infer conclusions on pH state and trends.

In fact, several regression relationships have been proposed for the Mediterranean Sea (Schneider et al., 2007; Copin-Montegut, 1993) and indicate different reconstructions. In addition, regressions based on local areas exist (Santana-Casiano et al., 2002;

BGD
11, 12871–12893, 2014

Huertas et al., 2009), some of which indicate a negative correlation between alkalinity and salinity in regions of freshwater (river) input (Luccheta et al., 2010).

Processes based on numerical models represent an alternative to the use of empirical regressive models. In these models, alkalinity and dissolved inorganic carbon (DIC) are considered explicit state variables (master variables used to solve the carbonate system) that are transported by physical processes and interact with chemical and biological processes (Wakelinken et al., 2012; Prowe et al., 2009; Artioli et al., 2012; Turi et al., 2013; Fiechter et al., 2014). Additionally, this choice is not free from criticalities, as it implies the need to explicitly parameterize the major known relationships among DIC, alkalinity and the biogeochemical processes to define exactly which chemical compounds are considered in the definition of the alkalinity. The boundary and initial conditions of the area considered must also be estimated. The advantage of this approach is that once a numerical model exists, it can be used to make projections on future states.

Many studies were carried out to numerically simulate the carbonate system in the global oceans (Orr et al., 2005). In the Mediterranean Sea, the only modeling estimates were made by d'Ortenzio et al. (2008), who used an array of decoupled 1-D water column biogeochemical models forced by satellite observations.

In this manuscript, we upgrade an existing state-of-the-art biogeochemical model of the Mediterranean Sea (Lazzari et al., 2012) by adding the dynamics of the carbonate systems. We also use the extended model to integrate, in a coherent framework, the few available measures of carbonate system properties within the Mediterranean Sea and along its boundaries to derive a space–time climatology of alkalinity. The model results are then used to explore the space–time variability of this important parameter and assess its correlation with salinity.

BGD
11, 12871–12893, 2014

2 Model and data for the Mediterranean Sea

2.1 Biogeochemical and carbonate system coupled model

The biogeochemical modelling system of the Mediterranean Sea (OPATM-BFM) used in the present study is a 3-D transport reaction model. It is capable of resolving the large-scale variability and seasonal cycle of nutrients and primary producers (Lazzari et al., 2012).

The transport of dissolved and particulate matter is resolved using the OPATM transport model (Lazzari et al., 2010), offline forced by dynamic field that is reproduced by the hydrodynamic general circulation model MED16 OGCM (Béranger et al., 2005). The transport is computed with a horizontal resolution of 1/8° (approximately 12 km) and with a vertical z-coordinate discretization that is coarser at the bottom layers and more refined at the surface layers (13 levels in the 0–200 m layer, 7 layers in the 200–600 m layer and 23 levels in the 600-bottom layer).

The dynamics of the biogeochemical properties are described by the BFM model (Vichi et al., 2007), a biogeochemical model that describes the cycles of nitrogen, phosphorus, silica and carbon through biotic (4 phytoplankton pools, heterotrophic bacteria, 2 microzooplankton, and 2 mesozooplankton pools) and abiotic (detritus, labile, semi-labile and refractory dissolved organic matter, dissolved inorganic compounds) components as a function of temperature and light.

The OPATM-BFM was upgraded by implementing a carbonate system module that considers two new state variables: dissolved inorganic carbon (DIC) and alkalinity.

DIC evolution is driven by the biological processes of photosynthesis and respiration and by the physical process of exchanges at air–sea interface. According to its explicit conservative expression (Wolf-Gladrow et al., 2007), the total alkalinity dynamic is affected by the biological processes that alter the concentrations of NO_3^-, PO_4^{3-} and NH_4^+. Nitrification, NH_4^+ uptake and the release of both NO_3^- and PO_4^{3-} decrease alkalinity by an equivalent amount of moles, whereas denitrification, the uptake of NO_3^- and

BGD
11, 12871–12893, 2014

PO_4^{3-} and NH_4^+ release increase alkalinity (Wolf-Gladrow et al., 2007). DIC exchange at the air–sea interface is solved by computing the seawater pH, pCO_2 and gas transfer formula, following the OCMIP II formulations (Orr et al., 1999). The evaporation-precipitation flux at the surface, which affects alkalinity and DIC by producing either a concentration or a dilution, is also considered.

2.2 Model setup

The present run covers the 1999–2004 period; the physical and biogeochemical setups are extensively detailed by Béranger et al. (2005) and Lazzari et al. (2012) and are briefly reported here. The atmospheric forcings are from the ERA40 reanalysis (Uppala et al., 2005), and from the ECMWF analysis. The initial conditions of physical variables are based on the MODB4 climatology (Brankart and Brasseur, 1998), and those of the nutrients are based on the Medar-Medatlas datasets (Crise et al., 2003). The nutrient loads (nitrates, phosphates and silicates) are from the terrestrial inputs derived from the paper of Ludwig et al. (2009). The atmospheric inputs of phosphates and nitrates are also included, considering a mean annual value for the eastern and western Mediterranean Sea (Ribera d'Alcalà et al., 2003). A buffer zone in the Atlantic zone is used to simulate the boundary at the Strait of Gibraltar, as detailed by Béranger et al. (2005) and Lazzari et al. (2012).

Regarding the new variables related to the carbonate system, three mean profiles are computed from Meteor51 (Table 2) and used to uniformly initialize the western Mediterranean Sea (alb, nwm, sww, swe and tyr sub-basins in Fig. 1), Ionian-Adriatic Seas (ion, adn and ads in Fig. 1) and Levantine (lev in Fig. 1). The Aegean Sea (aeg) is initialized with a mean profile that is computed from the Sesame-Aegean dataset (Table 2). A Newtonian dumping term regulates the Atlantic buffer zone that is outside the Strait of Gibraltar, where the alkalinity and DIC concentrations are relaxed to the mean profiles derived from the data published by Huertas et al. (2009) and Dafner et al. (2001).

BGD
11, 12871–12893, 2014

The terrestrial inputs of alkalinity are computed as the products of freshwater flows, as given by Ludwig et al. (2009), and the terrestrial concentration of alkalinity per water mass, estimated from each of the 10 macro coastal sectors used by Ludwig et al. (2009), based on previously obtained data (Copin-Montégut, 1993). Table 1 reports the mean alkalinity values at the macro coastal areas and the annual loads, including the quota of the most relevant rivers. The Dardanelles inputs are considered in the same way but based on previous information (Somot et al., 2008; Copin-Montégut, 1993). Atmospheric CO_2 is set according to the trend shown at the Lampedusa station (Artuso et al., 2009).

To smooth artificial effects of discontinuous initial conditions, before launching the actual biogeochemical simulation a spin up period was run by using meteo forcing typical of the period.

2.3 Reference dataset for comparison

A reference dataset of alkalinity observations (Table 2) has been gathered for model initialization and validation. The dataset consists of more than 4200 alkalinity measurements gathered in several campaigns and research cruises (Table 2) in the 1999–2011 period. Given the inhomogeneity and sparsity of the space and time of data, the average climatology profiles have been computed for a grid of $1^\circ \times 1^\circ$ for the year and the four seasons. The $1^\circ \times 1^\circ$ bins at any given quota are considered empty when at least one the two following conditions are met: fewer than 4 measurements were present, or the value of coefficient of variation was larger than 40 %.

BGD
11, 12871–12893, 2014

3 Results

3.1 Spatial variability of alkalinity

The physical and biogeochemical results of the present simulation have been extensively presented and validated by Béranger et al. (2005) and Lazzari et al. (2012). Here, we focus on the alkalinity time and space variability in the Mediterranean Basin.

The results show that the Mediterranean Sea is characterized by alkalinity values that are much higher (100–150 µmol kg^{-1} higher) than those observed in the Atlantic Ocean at the same latitude (Lee et al., 2006). The results indicate a strong surface west-to-east gradient (Fig. 2a), with values ranging from 2400 µmol kg^{-1} near the Strait of Gibraltar to 2700 µmol kg^{-1}, as simulated in the upper ends of the eastern marginal seas (Adriatic and Aegean Seas). The west-to-east gradient is a permanent structure along the water column (Fig. 2), although its strength becomes less marked in the maps of the intermediate and deep layers. Indeed, the range of variability of alkalinity for the deepest layer spans from 2560 µmol kg^{-1} of the Alboran Sea to 2620 µmol kg^{-1} of the Levantine sub-basin (2650–2670 µmol kg^{-1} in the deeper layers of the Adriatic and Aegean Seas).

At the surface, alkalinity dynamics are driven by three major factors: the input in the eastern marginal seas (the terrestrial input from Po and other Italian rivers and the input from the Dardanelles, see Table 1), the effect of evaporation in the eastern basin and the influx of the low alkaline Atlantic water. The thermohaline basin wide circulation modulates the intensity and the patterns of the spatial gradients. Intermediate and deep layers show lower dynamics and less variability. The Adriatic and Aegean Seas recharge the Levantine intermediate and deep waters: the dense water formation processes drive the downwelling of the high alkaline surface water, which then spreads from the eastern towards the western sub-basins.

The model reconstructions of horizontal gradients at the different depths are quite consistent with the reference values (Fig. 2). High correlation values and low relative root mean square error values (depicted in the Taylor diagram of Fig. 3) quantitatively

BGD
11, 12871–12893, 2014

confirm the good performance of the model in reproducing the mean annual fields. Higher relative errors (normalized bias and RMSE) are registered at the deepest layers (Figs. 2d and 3e), where the effect of input of high alkaline water from the Aegean and Adriatic to the Ionian Sea and Levantine regions appears to be partly underestimated. However, considering the absolute values, the bias and RMSE are quite low: 10.4 µmol kg^{-1} and 14.6 µmol kg^{-1}, respectively. These values are significant only because of the low variability in these layer (standard deviation equals to 15.8 µmol kg^{-1}).

3.2 Alkalinity vs. salinity regression

It has been recognized that several relationships between alkalinity and salinity are appropriate for different sub-basins of the Mediterranean Sea, given the different sources of alkalinity and water mass dynamics (Schneider et al., 2007; Touratier and Goyet, 2011; Luchetta et al., 2010). The results of the present run allow for the basin-wide quantification of these regressions and an investigation of the rationale of their differences (Fig. 4).

The relationship computed using the model grid points of the offshore areas (points with depths greater than 200 m) is similar to that obtained by Schneider et al. (2007), which permits the conclusion that at a basin scale, the effect of evaporation and the end term of Atlantic water are the major drivers for alkalinity dynamics. However, this regression is the average of two regressions: one computed for the eastern sub-basins (ion and lev) and one computed for the western sub-basins (alb, tyr, sww and swe), showing that the two sub-basins are affected by different sources of interference. The western regression has a higher correlation and lower dispersion values for residuals and lower regression coefficient values compared with the eastern sub-basin, highlighting that the latter sub-region is characterized by the presence of more intense sources of variability. In fact, significant deviations from the Mediterranean relationship exist for the eastern marginal seas (Adriatic and Aegean Seas). Here, input from rivers and the Dardanelles trigger a negative correlation between salinity and alkalinity. The Adriatic Sea regression shows the highest dispersion in coefficient values and error of residu-

BGD
11, 12871–12893, 2014

als as a consequence of the higher variability generated by the local and topographic effects in this elongated sub-basin. Further, for the nwm sub-basin, the effect of inputs from Rhone and Ebro rivers generate a negative correlation, but this effect remains confined only in the Gulf of Lion. Other local effects can produce deviations from the general relationship, as for example, the coastal areas of the Gulf of Gabes and the far eastern coastal area of the Levantine sub-basin, where local sources of terrestrial inputs are associated with high rates of evaporation flux and thus produce the clusters of orange and red points lying above the Mediterranean Sea regression (dashed thick line).

3.3 Seasonal temporal variability of alkalinity profiles

Vertical profiles are generally characterized by minimum values between the surface and 100 m, a sharp increase until 200–250 m and almost stationary values below 400–500 m (Fig. 5), but important differences between the eastern and western profiles highlight the presence of different forcings, water mass dynamics and confinements that characterize the Mediterranean Sea.

A marked seasonal cycle is depicted in the surface layer, whereas the deeper layers (i.e., below 200–250 m) show less temporal variability throughout the year. The mean annual variation of surface alkalinity ranges from approximately 10–40 $\mu mol\,kg^{-1}$, depending on the area of the Mediterranean Sea, due to both physical and biological processes. The extent of seasonal variability is consistent with available observations, as shown by the high values of the skill indexes depicted in the Taylor diagram for the seasonal comparison (symbols in Fig. 3).

The largest fluctuations are observed in the transition areas between the coastal zone and the open sea (Fig. 5a) and in the transition areas between different sub-basins (point d and e), where the surface circulation modifies the patterns of the horizontal gradients. In the Levantine and Ionian sub-basins, the seasonal cycle of summer evaporation and winter mixing produces a mean seasonal variability of more than 30 $\mu mol\,kg^{-1}$ in the first 50–100 m (Fig. 5g and h). The balance between surface

BGD
11, 12871–12893, 2014

evaporation and precipitation, which is generally positive for the Mediterranean Sea, contributes to increasing the surface alkalinity, with an average rate that ranges from 0.5–1 μmol m^{-2} d^{-1} in the western sub-basins to 1–2.5 μmol m^{-2} d^{-1} in the eastern sub-basins.

The intense vertical mixing in the Gulf of Lion (Fig. 5a), where the periodical ocean convection brings deep waters to the surface and is characterized by high alkalinity values, produces a more straight profile throughout the year compared with other areas.

In the southwest Mediterranean Sea (point c and d), the mixing of Levantine water (below 400 m) and the Atlantic water (upper layer) generates a zone (between 150 and 400 m) that is characterized by large temporal variability. Moving eastward, at points e and f, the modified Atlantic water generates a minimum at 50–100 m in the summer, when stratification confines the increase in alkaline concentration due to the evaporation effect to the surface layer. Below the modified Atlantic water, the intermediate Levantine water is characterized by alkalinity values of 2610–2620 μmol kg^{-1}. This layer is recharged by the high alkalinity values and dense water that are generated in the Adriatic and Aegean Seas and subsequently deepens in the Levantine and Ionian sub-basins.

In the surface layers of the water column, biological processes significantly contribute to the annual variability (red and blue shaded areas in Fig. 5). The biological contribution is calculated as the rate of change of μmol kg^{-1} $year^{-1}$ for the winter (from January to June) and summer (from July to December) seasons. The largest impact of biology is in the nwm region (Fig. 5a). The high rate of plankton production causes a large uptake of NO_3^- and PO_4^{3-} (which exceed the NH_4^+ uptake) during the first half of the year (blue areas), triggering an increase of alkalinity that can be higher than 0.10 μmol m^{-3} d^{-1} in the first 50–100 m of the water column. During summer, the productivity decreases (Lazzari et al., 2012), and in the layer below 100–120 m, the mineralization of NO_3^- (thought processes of mineralization of NH_4^+ and subsequent nitrification) and PO_4^{3-} generally prevails. At these depths, biology contributes negatively to alkalinity throughout the year even if at very low rate. The relevance of biological processes in contribut-

BGD
11, 12871–12893, 2014

ing to the alkalinity dynamics decreases from the northwestern to the eastern regions, according to the well-known decrease in the Mediterranean trophic gradient (Lazzari et al., 2012). The depth at which the positive impact of biology on alkalinity becomes zero increases as one moves eastward from 80–100 m (Fig. 5a and d) to 120 m of the eastern sub-basins (Fig. 5g), according to the deepening of the deep chlorophyll maximum from west to east. Therefore, it appears that biology contributes to the high temporal variability of the surface values in the western sub-basins and that, together with physical processes, it contributes to the increase in alkalinity with depth in the eastern sub-basins.

4 Conclusions

In this paper, we used a calibrated state-of-the-art 3-D transport-biogeochemical-carbonate model to integrate the experimental observations of alkalinity collected over the last decade into a single picture. The model results return a coherent picture of the space–time evolution of this parameter, which is crucial for properly assessing the impacts of ocean acidification and can help us understand how different factors (e.g., Atlantic water ingression, input from rivers and marginal seas, evaporation, physical transport, biogeochemical processes) contribute to defining spatial gradients and seasonal variation in alkalinity. The results present a basin-wide estimate of alkalinity, a contribution to the global alkalinity compilation, and a sound reference point for assessing model projections of the future state under climatic scenarios. The model results also show how the regression between salinity and alkalinity strongly varies from region to region and highlight that it is possible to use a single equation to reconstruct alkalinity values over the whole Mediterranean Sea only if marginal seas and regions of freshwater influence are not considered. The regression equations for each of these regions, treated separately, were also computed.

Acknowledgements. This study was supported by the EU projects MEDSEA (grant agreement n. 265103) and OPEC (grant agreement n. 283291).

BGD
11, 12871–12893, 2014

References

Artioli, Y., Blackford, J. C., Butenschon, M., Holt, J. T., Wakelin, S. L., Thomas, H., Borges, A. V., and Allen, J. I.: The carbonate system in the North Sea: sensitivity and model validation, J. Marine Syst., 102–104, 1–13, 2012.

Artuso, F., Chamard, P., Piacentino, S., Sferlazzo, D. M., De Silvestri, L., di Sarra, A., Meloni, D., and Monteleone, F.: Influence of transport and trends in atmospheric CO_2 at Lampedusa, Atmos. Environ., 43, 3044–3051, 2009.

Bégovic, M. and Copin, C.: Alkalinity and pH measurements on water bottle samples during THALASSA cruise PROSOPE, doi:10.1594/PANGAEA.805265, 2013.

Béranger, K., Mortier, L., and Crèpon, M.: Seasonal variability of water transport through the Straits of Gibraltar, Sicily and Corsica, derived from a high-resolution model of the Mediterranean circulation, Prog. Oceanogr., 66, 341–364, 2005.

Brankart, J.-M. and Brasseur, P.: The general circulation in the Mediterranean Sea: a climatological approach, J. Marine Syst., 18, 41–70, 1998.

Copin-Montégut, C.: Alkaninity and carbon budgets in the Mediterranean, Global Biogeochem. Cy., 7, 915–925, 1993.

Copin-Montégut, C. and Bégovic, M.: Carbonate properties and oxygen concentrations at time series station DYFAME D, doi:10.1594/PANGAEA.738581, 2002.

Crise, A., Solidoro, C., and Tomini, I.: Preparation of initial conditions for the coupled model OGCM and initial parameters setting, MFSTEP report WP11, subtask 11310, 2003, 2003.

Dafner, E., Gonzalez-Davila, M., Santana-Casiano, J. M., and Sempere, R.: Total organic and inorganic carbon exchange through the Strait of Gibraltar in September 1997, Deep-Sea Res. Pt. I, 48, 1217–1235, 2001.

d'Ortenzio, F., Antoine, D., and Marullo, S.: Satellite-driven modeling of the upper ocean mixed layer and air–sea CO_2 flux in the Mediterranean Sea, Deep-Sea Res. Pt. I, 55, 405–434, 2008.

Fiechter, J., Curchitser, E. N., Edwards, C. A., Chai, F., Goebel, N. L., and Chavez, F. P.: Air–sea CO_2 fluxes on the California Current: impacts of model resolution and coastal topography, Global Biogeochem. Cy., 28, 371–385, 2014.

Huertas, I. E.: Hydrochemistry measured on water bottle samples during Al Amir Moulay Abdallah cruise CARBOGIB-1. Unidad de Tecnología Marina – Consejo Superior de Investigaciones Científicas, doi:10.1594/PANGAEA.618900, 2007a.

BGD
11, 12871–12893, 2014

Huertas, I. E.: Hydrochemistry measured on water bottle samples during Garcia del Cid cruise GIFT-1. Unidad de Tecnología Marina – Consejo Superior de Investigaciones Científicas, doi:10.1594/PANGAEA.618916, 2007b.

Huertas, I. E., Ríos, A. F., García-Lafuente, J., Makaoui, A., Rodríguez-Gálvez, S., Sánchez-Román, A., Orbi, A., Ruíz, J., and Pérez, F. F.: Anthropogenic and natural CO_2 exchange through the Strait of Gibraltar, Biogeosciences, 6, 647–662, doi:10.5194/bg-6-647-2009, 2009.

Lazzari, P., Teruzzi, A., Salon, S., Campagna, S., Calonaci, C., Colella, S., Tonani, M., and Crise, A.: Pre-operational short-term forecasts for Mediterranean Sea biogeochemistry, Ocean Sci., 6, 25–39, doi:10.5194/os-6-25-2010, 2010.

Lazzari, P., Solidoro, C., Ibello, V., Salon, S., Teruzzi, A., Béranger, K., Colella, S., and Crise, A.: Seasonal and inter-annual variability of plankton chlorophyll and primary production in the Mediterranean Sea: a modelling approach, Biogeosciences, 9, 217–233, doi:10.5194/bg-9-217-2012, 2012.

Lee, K., Tong, L. T., Millero, F. J., Sabine, C. L., Dickson, A. G., Goyet, C., Park, G.-H., Wanninkhof, R., Feely, R. A., and Key, R. M.: Global relationships of total alkalinity with salinity and temperature in surface waters of the world's oceans, Geophys. Res. Lett., 33, L19605, doi:10.1029/2006GL027207, 2006.

Luchetta, A., Cantoni, C., and Catalano, G.: New observations of CO_2 -induced acidification in the northern Adriatic Sea over the last quarter century, Chemistry and Ecology, 26, 1–17, 2010.

Ludwig, W., Dumont, E., Meybeck, M., and Heussne, S.: River discharges of water and nutrients to the Mediterranean and Black Sea: major drivers for ecosystem changes during past and future decades?, Prog. Oceanogr., 80, 199–217, doi:10.1016/j.pocean.2009.02.001, 2009.

Orr, J. C., Najjar, R., Sabine, C. L., and Joos, F.: Abiotic HOWTO, Internal OCMIP Report, LSCE/CEA Saclay, Gifsur-Yvette, France, 1999.

Orr, J. C., Fabry, V. J., Aumont, O., Bopp, L., and Doney, S. C. Feely, R. A., Gnanadesikan, A., Gruber, N., Ishida, A., Joos„ F., Key, R. M., Lindsay, K., Maier-Reimer, E., Matear, R., Monfray, P., Mouchet, A., Najjar, R. G., Plattner, G.-K., Rodgers, K. B., Sabine, C. L., Sarmiento, J. L., Schlitzer, R., Slater, R. D., Totterdell, I. J., Weirig, M.-F., Yamanaka, Y., and Yool, A.: Anthropogenic ocean acidification over the twenty-first century and its impact on calcifying organisms, Nature, 437, 681–686, 2005.

BGD
11, 12871–12893, 2014

Prowe, F. A. E., Thomas, H., Pätsch, J., Kühn, W., Bozec, Y., Schiettecatte, L.-S., Borges, A. V., and de Baar, H. J. W.: Mechanisms controlling the air–seaCO_2 flux in the North Sea, Cont. Shelf. Res., 29, 1801–1808, 2009.
Ribera d'Alcalà, M., Civitarese, G., Conversano, F., and Lavezza, R.: Nutrient ratios and fluxes hint at overlooked processes in the Mediterranean Sea, J. Geophys. Res., 108, 8106, doi:10.1029/2002JC001650, 2003.
Rodrigues, L. C., van den Bergh, J. C. J. M., and Ghermandi, A.: Socio-economic impacts of ocean acidification in the Mediterranean Sea, Mar. Policy, 38, 447–456, 2013.
Santana-Casiano, J. M., Gonzalez-Davila, M., and Laglera, L. M.: The carbon dioxide system in the Strait of Gibraltar, Deep-Sea Res. Pt. II, 49, 4145–4161, 2002.
Schneider, A., Wallace, D. W. R., and Kortzinger, A.: The alkalinity of the Mediterranean Sea, Geophys. Res. Lett., 34, L15608, doi:10.1029/2006GL028842, 2007.
Somot, S., Sevault, F., Déqué, M., and Crépon, M.: 21st century climate change scenario for the Mediterranean using a coupled atmosphere–ocean regional climate model, Global Planet. Change, 63, 112–126, 2008.
Tanhua, T., Alvarez, M., and Mintrop, L.: Carbon Dioxide, Hydrographic, and Chemical Data Obtained During the R/V Meteor MT84_3 Mediterranean Sea Cruise (April 5–April 28, 2011)., http://cdiac.ornl.gov/ftp/oceans/CLIVAR/Met_84_3_Med_Sea/. Carbon Dioxide Information Analysis Center, Oak Ridge National Laboratory, US Department of Energy, Oak Ridge, Tennessee, doi:10.3334/CDIAC/OTG.CLIVAR_06MT20110405, 2012
Touratier, F. and Goyet, C.: Impact of the eastern Mediterranean Transient on the distribution of anthropogenic CO_2 and first estimate of acidification fro the Mediterranean Sea, Deep-Sea Res. Pt. I, 58, 1–15, 2011.
Turi, G., Lachkar, Z., and Gruber, N.: Spatiotemporal variability and drivers of pCO_2 and air–sea CO_2 fluxes in the California Current System: an eddy-resolving modeling study, Biogeosciences, 11, 671–690, doi:10.5194/bg-11-671-2014, 2014.
Turley, C. and Boot, K.: The ocean acidification challenges facing science and society, in: Ocean Acidification, edited by: Gattuso, J.-P. and Hansson, L., Oxford University Press, 249–271, 2011.
Uppala, S. M., Kallberg, P. W., Simmons, A. J., Andrae, U., da Costa Bechtold, V., Fiorino, M., Gibson, J. K., Haseler, J., Hernandez, A., Kelly, G. A., Li, X., Onogi, K., Saarinen, S., Sokka, N., Allan, R. P., Andersson, E., Arpe, K., Balmaseda, M. A., Beljaars, A. C. M., van de Berg, L., Bidlot, J., Bormann, N., Caires, S., Chevallier, F., Dethof, A.,

BGD
11, 12871–12893, 2014

Dragosavac, M., Fisher, M., Fuentes, M., Hagemann, S., Holm, E., Hoskins, B. J., Isaksen, L., Janssen, P. A. E. M., Jenne, R., McNally, A. P., Mahfouf, J.-F., Morcrette, J.-J., Rayner, N. A., Saunders, R. W., Simon, P., Sterl, A., Trenberth, K. E., Untch, A., Vasiljevic, D., Viterbo, P., and Woollen, J.: The ERA-40 re-analysis, Quart. J. R. Meteorol. Soc., 131, 2961–3012, 2005.

Vichi, M., Pinardi, N., and Masina, S.: A generalized model of pelagic biogeochemistry for the global ocean ecosystem, Part I: Theory, J. Marine Syst., 64, 89–109, 2007.

Zeebe, R. E. and Wolf-Gladrow, D.: CO_2 in Seawater: Equilibrium, Kinetics, Isotopes, Elsevier Oceanography Series, Elsevier, Amsterdam (NL), 2001.

Wakelin, S. L., Holt, J. T., Blackford, J. C., Allen, J. I., Butenschön, M., and Artioli, Y.: Modeling the carbon fluxes of the northwest European continental shelf: validation and budgets, J. Geophys. Res., 117, C05020, doi:10.1029/2011JC007402, 2012.

Wolf-Gladrow, D. A., Zeebe, R. E., Klaas, C., Körtzinger, A., and Dickson, A. G.: Total alkalinity: the explicit conservative expression and its application to biogeochemical processes, Mar. Chem., 106, 287–300, 2007.

BGD
11, 12871–12893, 2014

Table 1. Alkalinity concentration for each drainage basin and mean annual discharge from rivers and diffuse run-off from the given sub-basins. Values of [mmol Eq. m^{-3}] are derived from Copin-Montégut (1993).

Sub-basins and major rivers	Alkalinity [mmol m^{-3}]	Alkalinity discharges [Gmol y^{-1}]
Alboran (alb)	2960	12
southwest west (sww) and southwest east (swe)	2960	23
north west Mediterranean (nwm)	2960	251
– Ebro		31
– Rhone		163
Tyrrhenian Sea (tyr)	5675	104
northern Adriatic Sea (adn) and southern Adriatic Sea (ads)	2700	319
– Po		182
Ionian Sea (ion)	2200	36
Aegean Sea (aeg)	2620	1265
– Dardanelles		1150
Levantine (lev)	2200	79
– Nile		32

BGD
11, 12871–12893, 2014

Table 2. List of available alkalinity datasets for the Mediterranean Sea.

Name	Area	Period	Reference
Meteor51	Mediterranean Sea	Jun 2001	Schneider et al. (2007)
Meteor84	Mediterranean Sea	Apr 2011	Tanhua et al. (2012)
Prosope	Western Mediterranean and Ionian Sea	1999	Bégovic and Copin (2013)
Boum2008	Mediterranean Sea	Jun–Jul 2008	Touratier et al. (2012)
Sesame Egeo	Aegean Sea	Apr, Sep 2008	http://isramar.ocean.org.il/PERSEUS_Data
Sesame Regina Maris Sesame Garcia del cid	Alboran Sea	Apr, Sep 2008	http://isramar.ocean.org.il/PERSEUS_Data
Sesame Adriatic	Adriatic and northern Ionian Sea	Apr, Oct 2008	http://isramar.ocean.org.il/PERSEUS_Data
CARBGIB 1–6	Gibraltar Strait, Alboran Sea	2005–2006	Huertas (2007a)
GIFT1–2	Gibraltar Strait, Alboran Sea	2005–2006	Huertas (2007b)
Dyfamed	Gulf of Lions	2001–2005	Copin-Montégut and Bégovic (2002)

BGD
11, 12871–12893, 2014

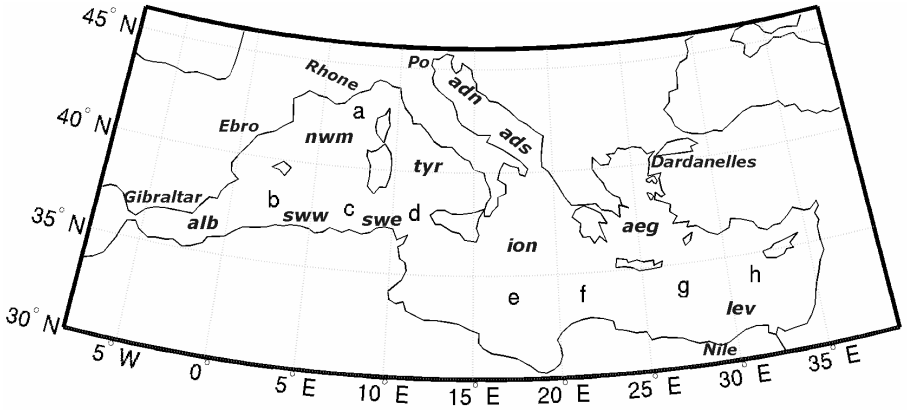

Figure 1. Map of the Mediterranean Sea reporting the sub-basins indication (alb, Alboran; nwm, northwest Med; sww, southwest west; swe, southwest east; tyr, Tyrrhenian Sea; ion, Ionian Sea; adn, northern Adriatic Sea; ads, southern Adriatic Sea; aeg, Aegean Sea; lev, Levantine), the location of principal rivers and boundaries and the coordinates of points (letters) of the profiles given in Fig. 4.

BGD
11, 12871–12893, 2014

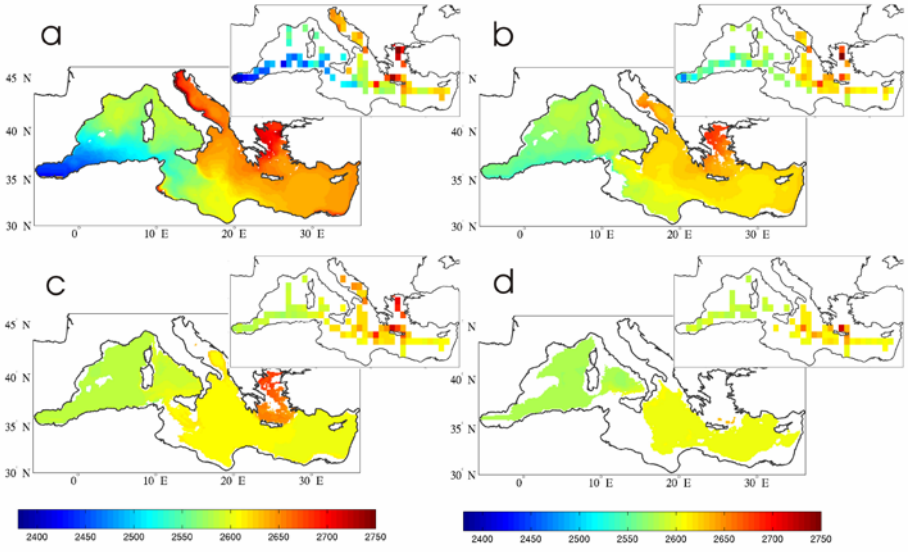

Figure 2. Alkalinity maps for selected layers: surface **(a)**, 100–200 m **(b)** 400–1500 m **(c)** 1500–4000 **(d)**. Model maps refer to the average of the simulation. Maps of 1° × 1° annual climatology are reported in the upper right corner of each selected layer.

BGD
11, 12871–12893, 2014

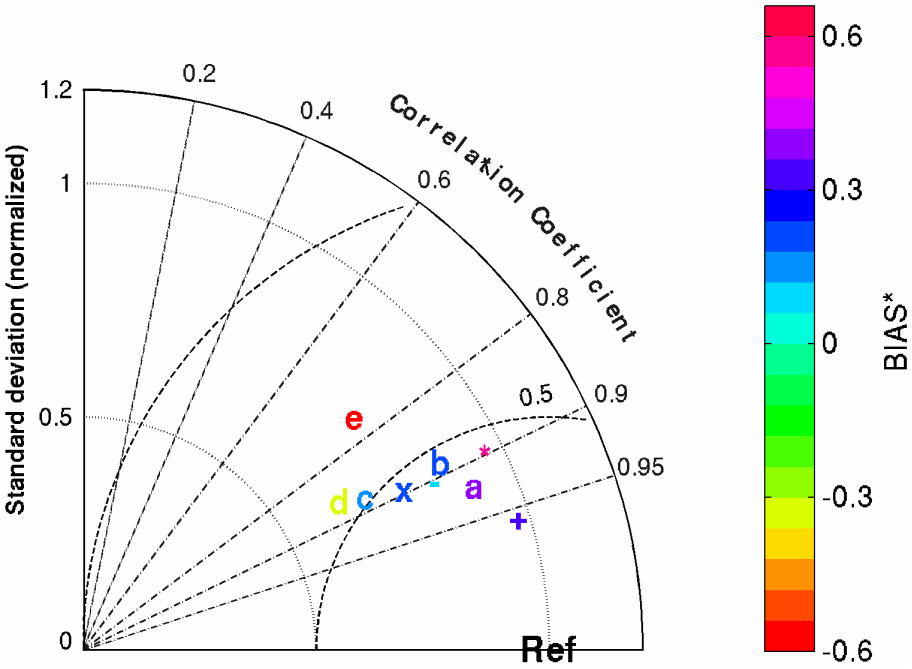

Figure 3. Taylor diagram of alkalinity of the mean annual model and observation fields for the following layers: surface **(a)**, 50–100 m **(b)**, 100–200 m **(c)**, 200–1500 m **(d)**, and 1500–4000 m **(e)** and for the following seasons at the surface layer: winter (+), spring (−) summer (x), autumn (*). The color bar reports the normalized bias (*BIAS = bias divided by the standard deviation of observations).

BGD
11, 12871–12893, 2014

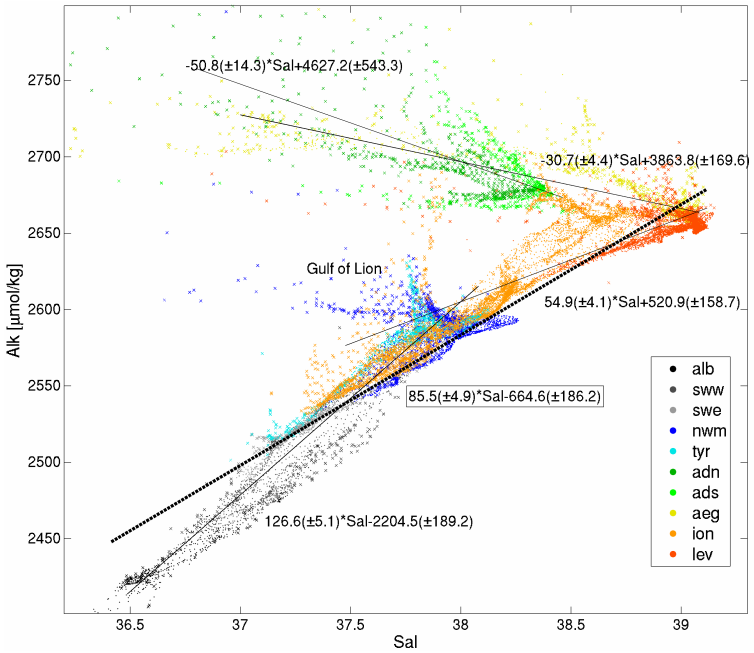

Figure 4. Regression between salinity and alkalinity at the surface. Colored points belong to the different sub-basins of Fig. 1. Regression for the Mediterranean Sea is shown by a dashed line, and the equation is reported in the black box (95 % confidence intervals of the coefficients are in brackets; $p < 0.001$; $R^2 = 0.91$; RMSD = 18.8). The regression uses data from the alb, sww, swe, tyr, ion, lev sub-basins with depths greater than 200 m. Sub-basin regressions are computed for the Adriatic sea (all data; $R^2 = 0.45$, RMSD = 32.0), the Aegean Sea (all data; $R^2 = 0.77$, RMSD = 9.3), the western Mediterranean Sea (data with depths greater than 200 m; $R^2 = 0.95$, RMSD = 11.6) and the eastern Mediterranean Sea (data with depths greater than 200 m; $R^2 = 0.74$, RMSD = 13.8).

BGD
11, 12871–12893, 2014

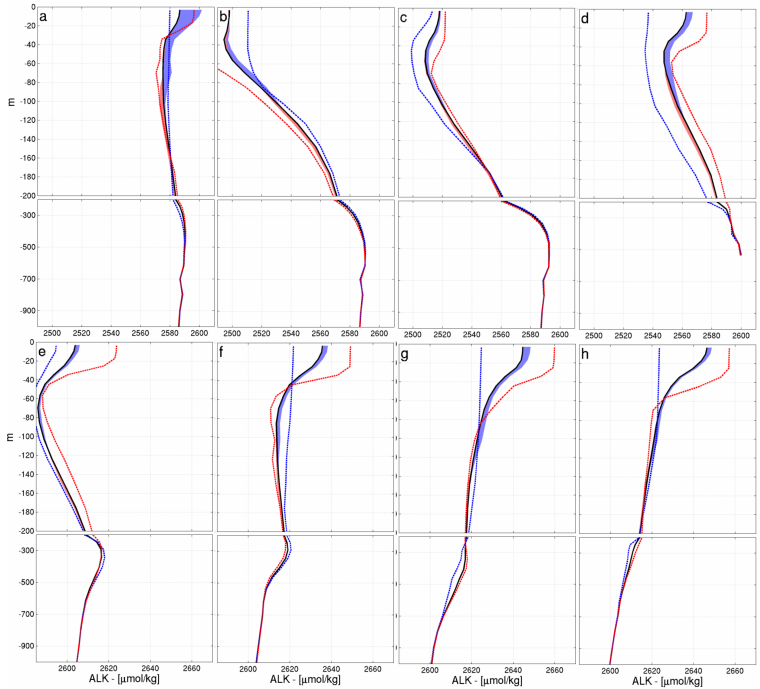

Figure 5. Mean vertical profiles of alkalinity (black line) in selected points of the Mediterranean Sea. Range of mean seasonal variability: winter (blue dashed line) and summer (red dashed line) profiles of maximum anomalies with respect to the mean annual profile. The mean annual rate of variation due to biological processes µmol kg^{-1} y^{-1} for winter (blue shaded area) and summer (red shaded area). The range of the x-axis changes for each point, but the labels always identify intervals of 20 µmol kg^{-1}.

BGD
11, 12871–12893, 2014